JOURNAL OF MAGNETIC RESONANCE IMAGING 31:1224–1229 (2010)

Technical Note

Improved Coronary MR Angiography Using Wideband Steady State Free Precession at 3 Tesla With Sub-millimeter Resolution

Hsu-Lei Lee, PhD,[1]* Ajit Shankaranarayanan, PhD,[2] Gerald M. Pohost, MD,[1,3] and Krishna S. Nayak, PhD[1,3]

Purpose: To suppress off-resonance artifacts in coronary artery imaging at 3 Tesla (T), and therefore improve spatial resolution.

Materials and Methods: Wideband steady state free precession (SSFP) sequences use an oscillating steady state to reduce banding artifacts. Coronary artery images were obtained at 3T using three-dimensional navigated gradient echo, balanced SSFP, and wideband SSFP sequences.

Results: The highest in-plane resolution of left coronary artery images was 0.68 mm in the frequency-encoding direction. Wideband SSFP produced an average SNR efficiency of 70% relative to conventional balanced SSFP and suppressed off-resonance artifacts.

Conclusion: Wideband SSFP was found to be a promising approach for obtaining noncontrast, high-resolution coronary artery images at 3 Tesla with reliable image quality.

Key Words: coronary artery imaging; balanced SSFP; wideband SSFP; alternating repetition time
J. Magn. Reson. Imaging 2010;31:1224–1229.

CORONARY ARTERY DISEASE is the leading cause of death in the Western world, and is responsible for approximately 450,000 deaths per year in the United States (1). For this reason, imaging of the coronary artery lumen (particularly lumenal narrowing) is one of the most critical applications of medical imaging. Compared with the current gold standard X-ray angiography, and emerging multi-slice computed tomography, coronary imaging with MR has the advantages of being noninvasive and involving no ionizing radiation. The most widely used MR coronary imaging protocols are based on segmented three-dimensional (3D) Fourier transform gradient acquisitions with cardiac gating and respiratory navigation, and have proved useful for the diagnosis of proximal disease and coronaries with anomalous origin (2). Reliable imaging of distal coronary segments remains an open problem, and may become possible with improvements in signal-to-noise ratio (SNR), contrast-to-noise ratio (CNR), and spatial resolution.

At 1.5 Tesla (T), balanced steady state free precession (SSFP, also known as True-FISP, FIESTA, or Balanced-FFE) imaging has been shown to provide significantly superior SNR and CNR compared with gradient echo sequences (3), and may alleviate the need for contrast agents as in the widely used slow-injection gradient echo imaging method (4). High-field MRI platforms can also lead to improved SNR, which is roughly proportional to the static magnetic field strength. In experimental coronary MR angiography studies, patient blood SNR using gradient echo sequences at 3T has been measured to be 30% higher than at 1.5T (5), and SSFP blood SNR at 3T has been measured to be 53% higher than at 1.5T (6).

The combination of SSFP and 3T has been used to generate coronary artery images with higher SNR and blood–myocardium CNR compared with 1.5T (7). However, SSFP imaging suffers from sensitivity to B_0 inhomogeneity (8–11). Susceptibility-induced resonance frequency shifts increase linearly with magnetic field strength and generate greater off-resonance artifact at higher B0 field strengths, resulting in degradation of SSFP image quality. This sensitivity is also proportional to the imaging repetition time (TR). To prevent off-resonance banding artifacts in SSFP imaging, the readout length must be constrained to maintain a short TR. Robust cardiac MRI at 3T demands an imaging bandwidth of 250 to 300 Hz to cover the range of resonance offsets across the human heart, which requires a TR no longer than 3.3 to 4 ms using

[1]Ming Hsieh Department of Electrical Engineering, University of Southern California, Los Angeles, California, USA.
[2]Global Applied Science Lab., GE Healthcare, Menlo Park, California, USA.
[3]Keck School of Medicine, University of Southern California, Los Angeles, California, USA.

Contract grant sponsor: National Institutes of Health; Contract grant number: R21-HL079987; Contract grant sponsor: American Heart Association; Contract grant number: 0435249N; Contract grant sponsor: James H. Zumberge Foundation; GE Healthcare.

*Address reprint requests to: H.-L.L., University Hospital Freiburg, Department of Radiology, Medical Physics, Breisacher Str. 60a, PH2a 79106 Freiburg, Germany. E-mail: hsu-lei.lee@uniklinik-freiburg.de

Received October 14, 2009; Accepted February 5, 2010.
DOI 10.1002/jmri.22150
Published online in Wiley InterScience (www.interscience.wiley.com).

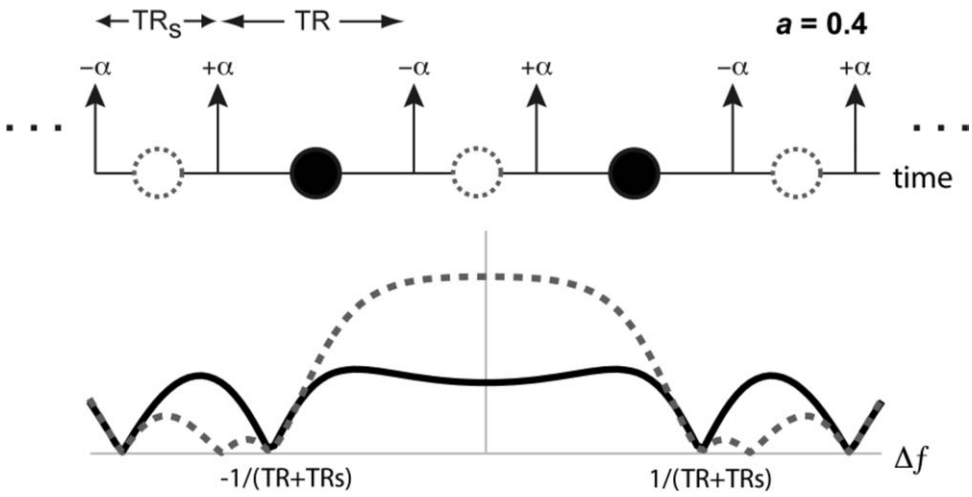

Figure 1. Wideband SSFP pulse sequence (top) and its spectral response (bottom). Black solid line represents the spectral response of the echo in TR (black circle); gray dotted line represents the spectral response of the echo in TR_s (gray dotted circle). The signal profiles are based on $a = TR_s$ / TR = 0.4, T_1/T_2 = 1500/140 ms, and $T_1, T_2 >> TR$.

conventional SSFP (12). For diagnostic-quality coronary artery imaging, sub-millimeter resolution is essential. The need for a short TR limits the usable readout duration given the gradient hardware limitations on commercial systems, and makes it difficult to achieve sub-millimeter resolution, thereby limiting the diagnostic value of resulting coronary artery images.

Alternating TR (ATR) methods have been recently developed as a means for modifying the spectral response of SSFP. This approach can be used with specific TR combinations and corresponding phase cycling to achieve fat suppression (13), or with 0-π phase cycling to widen the band spacing and relax the TR limitation (14). The latter approach, called wideband SSFP, allows for a flexible trade-off of the high SNR of 3T SSFP for increased band spacing in the spectral response of the sequence. It has been previously shown that, compared with conventional SSFP, wideband SSFP can suppress off-resonance related banding artifacts in steady-state cardiac imaging for a given spatial resolution (15). For a specific band spacing requirement, wideband SSFP increases the possible TR and thus the available readout duration, which improves the achievable spatial resolution.

In this work, we present the design and application of a wideband SSFP technique for sub-millimeter resolution coronary artery imaging at 3T. A 3D free-breathing respiratory navigated sequence was used with spectrally selective fat saturation. A scaled Kaiser ramp magnetization preparation scheme was used to stabilize the transient wideband SSFP signal. In healthy volunteers, we demonstrate that wideband SSFP provides a marked improvement in image quality and SNR, respectively, when compared with conventional SSFP and gradient echo sequences.

MATERIALS AND METHODS

Experimental Methods

Experiments were performed on a Signa Excite HD 3T scanner (GE Healthcare, Waukesha, WI). The gradient system had maximum amplitude 40 mT/m and maximum slew rate 150 mT/m/ms. The maximum receiver bandwidth was ±125 kHz (4 μs sampling). The body coil was used for radiofrequency (RF) transmission, and an eight-channel cardiac phased array was used for signal reception. Shimming was performed to minimize off-resonance artifacts, using the manufacturer provided automatic prescan, which is based on linear shimming of the central slice, followed by center frequency adjustment based on a region of interest placed across the heart. Scout images were then acquired to determine the precise center frequency to be used in coronary artery imaging (16). A second 2D cine scout scan aligned with the central slice in the 3D scan was performed, and the trigger delay of electrocardiograph (ECG) gating was chosen according to the mid-diastolic rest period observed in the cine series. Six healthy volunteers were scanned after providing written informed consent, and with an imaging protocol approved by our institutional review board. Wideband SSFP and balanced SSFP #1 scans were performed on all subjects, and additional balanced SSFP #2 and gradient echo scans were performed on three of the six subjects.

Increased Band Spacing Using Wideband SSFP

Wideband SSFP (14) uses two alternating repetition times (TR and TR_s) with alternating RF phase (0-π) to establish an oscillating steady state with two distinct echoes, as shown in Figure 1. The ratio of the short and long repetition times is defined as $a = TR_s$ /TR, where $0 < a <= 1$. This sequence has a null-to-null band spacing of approximately $2/(TR+TR_s)$, and the signal intensity decreases as the a-value is reduced. In this work, only the long TR is used for data acquisition.

Initial Preparation for Reducing Transient Oscillations

When starting at thermal equilibrium, the SSFP signal amplitude oscillates during the approach to steady state. The oscillation creates nonsmooth k-space weighting along the phase-encoding direction(s),

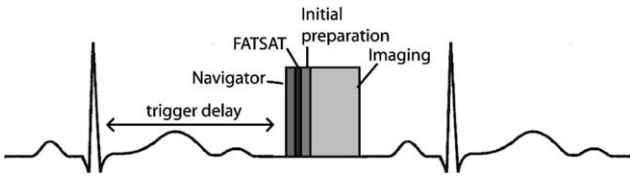

Figure 2. Pulse sequence for 3D coronary imaging. Each R-R interval consists of a pencil-beam navigator, fat saturation sequence, 16-cycle Kaiser-Bessel windowed ramp preparation, and imaging acquisitions centered at mid-diastole.

which results in image artifacts (17). The long waiting period before the signal reaches steady state degrades the effectiveness of important magnetization preparation schemes, such as fat saturation, T_2-preparation, and inversion recovery. Thus an efficient initial preparation is critical in noncontinuous scans (e.g., gated cardiac imaging).

Kaiser ramp method has been used for magnetization preparation in balanced SSFP coronary sequences (18). For wideband SSFP, a modified Fourier relationship between excitation flip angle increments and the resulting signal profile of alternating TR sequences has been derived using an approach similar to Le Roux's work on conventional SSFP (19), and a scaled Kaiser-Bessel preparation scheme was proposed to efficiently reduce transient signal fluctuation in wideband SSFP (20). In the proposed preparation scheme, the RF amplitude increments in TR and TR_s are scaled functions of the same Kaiser-Bessel window, with scale factors of a and 1, respectively. Before the 3D coronary artery scans, we compared the performance of the scaled Kaiser-Bessel preparation with dummy-cycle preparation in low-resolution breath-held left anterior descending (LAD) coronary artery imaging.

Imaging Sequence

Free-breathing coronary magnetic resonance images were acquired using a 3D respiratory navigated sequence with either a wideband SSFP, conventional SSFP or gradient echo acquisition. The pulse sequence structure is shown in Figure 2. A pencil-beam navigator over the right hemidiaphragm was acquired using the phased array coil before data acquisition in each cardiac cycle with a 5-mm acceptance window. After the navigator, a spectrally selective fat saturation pulse and dephaser gradient were applied. A 16-cycle Kaiser-Bessel ramp preparation was used to reduce transient oscillations in both wideband and conventional balanced SSFP, followed by image acquisition centered at mid-diastole. The acquisition window length was also determined based on the 2D cine scout scan, and was approximately 20% of the R-R interval. The 3DFT readouts were used with a sequential phase-encoding ordering and centric slice ordering (16–20 slices per slab). Scan parameters for the four different imaging protocols are listed in Table 1. The four scans were conducted in the order they appear in the table (left to right). For each subject, imaging TR was set to the minimum value considering the variant gradient slew rate limitation in individual oblique scan planes. The TR_s of wideband SSFP was chosen to maintain a null-to-null band spacing greater than 300 Hz. A centric slice order was used, to minimize the effect of prolonged scan time of wideband SSFP due to the currently unused TR_s period and avoid significant image quality loss.

SNR Efficiency of Wideband SSFP and Conventional SSFP

The total acquisition time of wideband SSFP is $(1 + a)$ times longer than conventional SSFP because only one k-space line is collected per $(TR+TR_s)$. The length of acquisition window in one R-R interval has to be kept within the diastolic rest period to avoid cardiac motion artifact, hence the total number of heart beats needed to obtain the same 3D volume is also increased by a factor of $(1 + a)$. To reduce the effect of the increased possibility of patient movement during a prolonged scan, we use a centric slice-encode ordering to acquire the center part of k-space at the beginning of the scan.

When only TR is used for imaging, the SNR efficiency of wideband SSFP, μ_w, can be written as:

$$\mu_w = \frac{\mu_c}{1+a} \times \frac{|M_{xy}|_w}{|M_{xy}|_c} \quad [1]$$

where $|M_{xy}|_w$ and $|M_{xy}|_c$ are the average signal intensity across 2/3 of the pass band of wideband SSFP and conventional SSFP, respectively, and μ_c is the SNR efficiency of conventional SSFP (13). As described

Table 1
In-Vivo Scan Parameters (Top) and Imaging Results (Bottom): SNR, Scan Time, and SNR Efficiency of 0.68 × 1.0 × 1.0 mm^3 Resolution Images Averaged Over Six Volunteer Scans

Sequence	Wideband SSFP	Balanced SSFP #1	Balanced SSFP #2	Gradient echo
TR (ms)	3.9 – 4.2	3.9 – 4.2	3.4 – 3.8	5.0 – 5.8
Flip Angle	55°	55°	55°	15°
Matrix Size	384 × 256	384 × 256	256 × 256	384 × 256
Spatial resolution (mm^3)	0.68 × 1.0 × 1.0	0.68 × 1.0 × 1.0	1.0 × 1.0 × 1.0	0.68 × 1.0 × 1.0
Band spacing (Hz)	≥300	238 – 256	~300	–
Navigator efficiency (%)	51.9 ± 5.1	49.0 ± 6.3	42.6 ± 7.6	49.9 ± 4.4
Scan time (min)	5.8 ± 0.7	4.8 ± 0.5	4.9 ± 0.1	5.5 ± 0.5
Aortic blood SNR	14.8 ± 3.2	19.1 ± 4.7	22.2 ± 4.8	7.3 ± 1.1
Aortic blood SNR efficiency	0.70 ± 0.15	1.0 ± 0.23	1.2 ± 0.3	0.36 ± 0.04

SNR = signal to noise ratio; SSFP = steady state free precession.

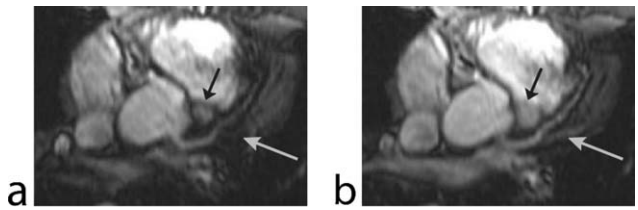

Figure 3. Wideband SSFP coronary artery images with different magnetization preparation methods. **a**: Dummy-cycles. **b**: Scaled Kaiser-Bessel ramp. The arrows indicate where the scaled Kaiser-Bessel ramp reduced artifacts and had better signal homogeneity.

in Eq. [1] of reference (14), $|M_{xy}|_w/|M_{xy}|_c$ is always less than 1, hence the SNR efficiency of wideband SSFP is always lower than that of conventional SSFP. Numerical simulations indicate that the 0.68 × 1.0 × 1.0 mm^3 resolution wideband SSFP coronary artery imaging sequence in this study should exhibit a theoretical blood SNR reduction of roughly 30% and an SNR efficiency reduction of roughly 45% compared with conventional SSFP.

After the LAD scans, regions of interest (ROIs) in the aorta (blood) and outside the body (background air) were manually selected in the high-resolution images. Blood SNR was defined as $SNR_{blood} = SI_{blood} / SD_{air}$, where the signal intensity (SI) of aortic blood pool and standard deviation (SD) of background noise were directly measured from the images. SNR efficiencies were calculated by dividing SNR values by the square root of total scan time, and were then normalized such that conventional SSFP images have a mean SNR efficiency of 1.0.

RESULTS

Figure 3 illustrates the influence of the wideband SSFP initial preparation scheme on final image quality. The figure contains two low-resolution LAD coronary artery images that were acquired in separate breath-holds using the same wideband SSFP imaging sequence, but with two different eight-cycle initial preparation schemes (a: dummy cycles and b: scaled Kaiser-Bessel ramp) (20). The image obtained with the scaled Kaiser-Bessel ramp shows reduced artifacts and more homogeneous blood signal intensity (see arrows). This example was shown for illustration; however, a 16-cycle Kaiser-Bessel ramp provided slightly more uniform signal in-vivo, and was used in all subsequent studies.

Figure 4 contains 3D reformatted LAD coronary artery images from three representative subjects. The four columns contain data from four separate navigated acquisitions: (i) wideband SSFP with 0.68 × 1.0 × 1.0 mm^3 spatial resolution, (ii) balanced SSFP #1 with the same spatial resolution and TR as column 1, (iii) balanced SSFP #2 with a band spacing similar to column 1 and 1.0 × 1.0 × 1.0 mm^3 spatial resolution, and (iv) gradient echo with the same spatial resolution as column 1.

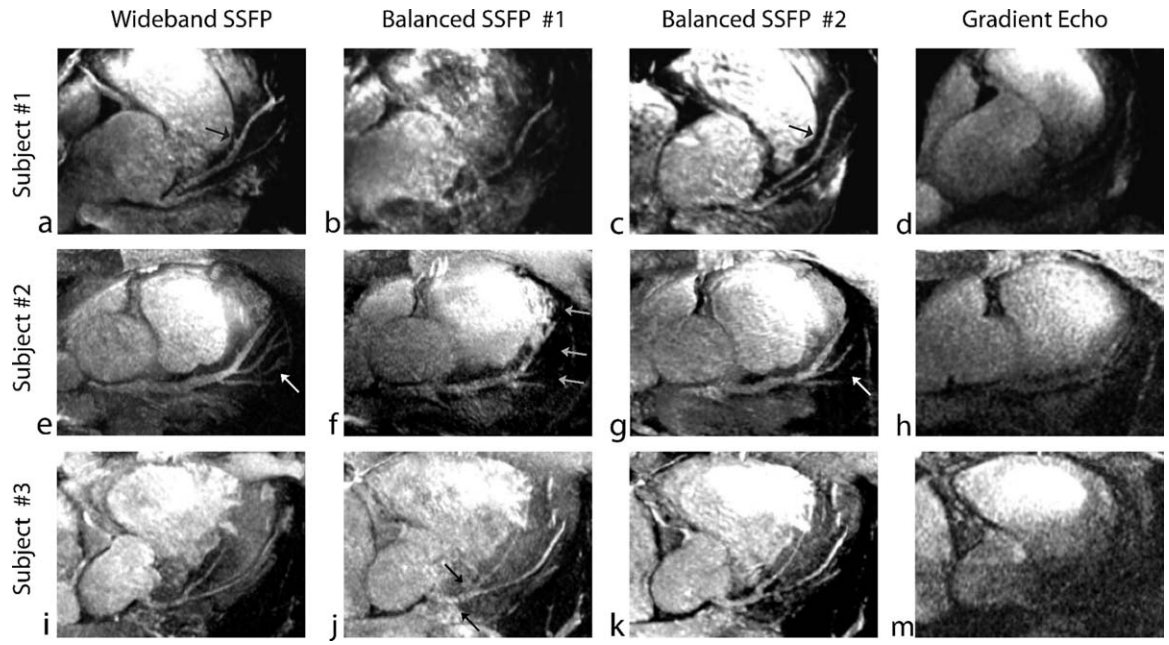

Figure 4. Left anterior descending coronary artery images from three representative subjects using four different imaging sequences (see Table 1). **a,e,i**: Wideband SSFP with 0.68 × 1.0 × 1.0 mm^3 spatial resolution. Average visible vessel length: 11.95±3.3 cm. **b,f,j**: Conventional balanced SSFP with 0.68 × 1.0 × 1.0 mm^3 spatial resolution. Average visible vessel length: 8.25±3.1 cm. **c,g,k**: Conventional balanced SSFP with 1.0 × 1.0 × 1.0 mm^3 spatial resolution. **d,h,m**: Gradient echo with 0.68 × 1.0 × 1.0 mm^3 spatial resolution. Each image is reformatted from a 3D slab acquisition. Wideband SSFP images provided the most uniform blood signal, and artifact free depiction of distal branches of the LAD. High resolution conventional SSFP suffers from off-resonance banding (f, see gray arrows) and flow-transient artifacts (b,j) that disrupt visualization of the coronary lumen. Low resolution conventional SSFP does not suffer from these artifacts but is unable to capture small distal branches (e versus a, see black arrows, and g versus e, see white arrows).

In all studies, wideband SSFP provided the most uniform blood signal, and artifact-free depiction of distal branches of the LAD (see Fig. 4a,e,i) with average visible vessel length of 11.95 ± 3.3 cm across all six subjects. Balanced SSFP suffered from substantial flow-related transient artifacts (see Fig. 4b,j) (12,21) that interfered with coronary assessment. With this sequence, the average visible vessel length was reduced to 8.25 ± 3.1 cm. Wideband SSFP and balanced SSFP with shorter TR did not suffer from these artifacts, presumably due to the wider null-to-null spacing in their spectral profile. Note that the high resolution balanced SSFP image of subject 2 (Fig. 4f) did not suffer from any noticeable flow artifact; however, dark bands appear in the mid-LAD region, and could confound image interpretation. Balanced SSFP with short TR was relatively artifact-free, but was not able to capture smaller branches due to the coarser spatial resolution (see white arrows in Fig. 4g versus Fig. 4e). In subject 3, the left main coronary artery in the balanced SSFP image was affected by the flow transient artifact (see black arrows in Fig. 4j). Wideband SSFP (Fig. 4i) avoided this artifact, but also suffered from reduced SNR. As a result, the mid- and distal-LAD were not as clearly depicted as in the balanced SSFP images. Gradient echo images (Fig. 4d,h,m) did not suffer from off-resonance banding artifact; however, the blood SNR was substantially lower than the alternatives.

The navigator efficiency, scan-time, blood SNR, blood SNR efficiencies from the four scans are summarized in Table 1. Navigator efficiencies ranged from 35.0% to 59.7% across the six subjects. The average blood SNR (measured in the aorta) of the wideband SSFP data was 22% lower than that of balanced SSFP data with the same spatial resolution. Considering the change in scan time, the average SNR efficiency of wideband SSFP was 70% of the SNR efficiency of conventional balanced SSFP.

DISCUSSION

We have designed, implemented, and evaluated a wideband SSFP-based method for 3D high-resolution free-breathing coronary artery imaging. In 0.68 × 1.0 × 1.0 mm^3 balanced SSFP scans, off-resonance banding and flow-related artifacts severely degraded the depiction of coronary arteries (Fig. 4b,f,j). Balanced SSFP with lower spatial resolution (and shorter TR) was able to avoid these artifacts but was not able to capture small and distal branches. Wideband SSFP was able to achieve 0.68 × 1.0 × 1.0 mm^3 spatial resolution with no visible artifacts and the most homogeneous blood signal intensity over the regions of interest. With TR/TR_s = 3.9/2.4 ms, wideband SSFP had a 24% wider null-to-null spacing in its spectral profile (~317 Hz) compared with conventional SSFP with the same TR.

The use of wideband SSFP involves a fundamental trade-off of SNR for spatial resolution and bandwidth. The balance between the three should be carefully evaluated to optimize image quality and the eventual ability to detect coronary artery disease (CAD) from images. This includes optimization of the TR, TR_s, bandwidth, and flip angle. It is worth noting that the reduction blood SNR in this study was less than the value predicted by Eq. [1]. Numerical simulations suggest that in the steady state blood SNR should be 30% lower when using wideband SSFP compared with balanced SSFP #1. The discrepancy could be due to inflow, which would mean that blood SNR is better modeled as a mix of various transient signals and partial T2-weighting. This would affect the choice of the imaging flip angle. It is likely that to maximize blood to myocardium contrast in the SSFP-based sequences, the flip angle should be set to the largest possible value within SAR constraints, because blood signal is always higher than that of myocardium and the difference increases with flip angle. The SAR of wideband SSFP is $2TR/(TR+TR_s)$ times that of balanced SSFP. Note that although the SAR of steady-state sequences is an important consideration in continuous imaging (e.g., CINE LV function), in the proposed coronary protocols, data is only collected during a stable diastolic window that certainly occupies ≤ 30% of each R-R interval. Thus, the SAR of imaging RF excitations is not a major limiting factor at 3T.

The total scan time for wideband SSFP is expected to increase by TR_s /TR compared with balanced SSFP #1, when the length of acquisition window is kept identical and TR_s is unused. In this study, the scan time increase was expected to be 50% to 60%, but in real scans it was only 24% on average, as a result of sequence restrictions on the number of *k*-space segments (which caused acquisition window length to vary during different scans), and also variations in the navigator efficiency. Therefore, the wideband SSFP approach achieved a 70% SNR efficiency compared with balanced SSFP, which was higher than the theoretical prediction of 55%.

Parallel imaging (22,23) was not used in this study, but can be easily incorporated as a means to shorten scan time, reduce the size of the acquisition window, and/or improve spatial coverage. It is possible for auto-calibrated parallel imaging methods (24) to obtain low-resolution coil sensitivity or *k*-space interpolator information during the TR_s (25), further reducing the required acquisition time. It may also be possible to acquire low-resolution data (e.g., 1-D projections) from the imaging volume during the short TR (26). Such data would provide direct information about the heart's position and could be used for self-gating (27) or automated detection of the stable diastolic window within a prolonged acquisition (28). No additional sequence or acquisition time would be needed to perform this procedure.

Many cardiac applications such as first pass perfusion (29) and global cardiac function imaging (30) benefit from higher field strengths, and the clinical use of cardiac MRI has begun to migrate toward 3T. Coronary artery imaging, as part of a comprehensive cardiac assessment, will also require a robust method to acquire high-quality artifact-free images at 3T. This study has demonstrated the ability of wideband SSFP to achieve sub-millimeter resolution while avoiding

banding artifacts that confound the use of conventional balanced SSFP at 3T. This approach should also have roughly 25% higher SNR efficiency compared with balanced SSFP at 1.5T, making it a promising candidate for noncontrast coronary MRA at 3T.

Wideband SSFP is a flexible pulse sequence, and this study represents its first application to coronary artery imaging. There are several opportunities for further development that include utilization of TR_s for improving SNR, navigation, self-gating, or auto-calibration for parallel imaging, and the optimization of imaging parameters or combination with T_2-prep (31) to further increase CNR. Further studies are needed to further develop this approach and determine the imaging parameters that will provide optimal image quality and optimal detection of CAD in clinical cohorts.

In conclusion, we have demonstrated a new approach to noncontrast, high-resolution coronary artery imaging at 3T, based on wideband SSFP. Compared with conventional balanced SSFP, this pulse sequence provided reduced sensitivity to off-resonance and permits prolonged readout duration. This directly led to the ability to achieve sub-millimeter resolution without the banding and flow-transient image artifacts that confound conventional balanced SSFP coronary artery imaging. Wideband SSFP retained superior SNR compared with gradient echo sequences. This work has provided an initial demonstration of the advantages of applying wideband SSFP to coronary artery imaging (higher resolution, reduced artifact) in healthy subjects. Further studies in patients are needed to determine imaging parameters that provide optimal image quality and optimal assessment of coronary artery disease with this new approach.

ACKNOWLEDGMENTS

We thank Maggie Fung for providing training on the use of respiratory navigators for coronary artery imaging. H.-L.L. has received support from a USC Viterbi School of Engineering Graduate Fellowship and a USC Women in Science and Engineering Merit Fellowship.

REFERENCES

1. Committee AHAS, Subcommittee SS. Heart disease and stroke statistics—2007 update. Circulation 2007;115:69–171.
2. Kim WY, Danias PG, Stuber M, et al. Coronary magnetic resonance angiography for the detection of coronary stenoses. N Engl J Med 2001;345:1863–1869.
3. Deshpande VS, Shea SM, Laub G, Simonetti OP, Finn JP, Li D. 3D magnetization-prepared True-FISP: a new technique for imaging coronary arteries. Magn Reson Med 2001;46:494–502.
4. Stuber M, Botnar RM, Danias PG, et al. Contrast agent-enhanced, free-breathing, three-dimensional coronary magnetic resonance angiography. J Magn Reson Imaging 1999;10: 790–799.
5. Sommer T, Hackenbroch M, Hofer U, et al. Coronary MR angiography at 3.0 T versus that at 1.5 T: initial results in patients suspected of having coronary artery disease. Radiology 2005;234: 718–725.
6. Bi X, Deshpande V, Simonetti O, Laub G, Li D. Three-dimensional breathhold SSFP coronary MRA: a comparison between 1.5 T and 3.0 T. J. Magn Reson Imaging 2005;22:206–212.
7. Stuber M, Botnar RM, Fischer SE, et al. Preliminary report on in vivo coronary MRA at 3 Tesla in humans. Magn Reson Med 2002; 48:425–429.
8. Carr HY. Steady-state free precession in nuclear magnetic resonance. Phys Rev 1958;112:1693–1701.
9. Oppelt A, Graumann R, Barfuss H, Fischer H, Hartl W, Shajor W. FISP – a new fast MRI sequence. Electromedica 1986;54:15–18.
10. Freeman R, Hill HDW. Phase and intensity anomalies in Fourier transform NMR. J Magn Reson 1971;4:366–383.
11. Zur Y, Stokar S, Bendel P. An analysis of fast imaging sequences with steady-state transverse magnetization refocusing. Magn Reson Med 1988;6:175–193.
12. Schär M, Kozerke S, Fischer SE, Boesiger P. Cardiac SSFP imaging at 3 Tesla. Magn Reson Med 2004;51:799–806.
13. Leupold J, Hennig J, Scheffler K. Alternating repetition time balanced steady state free precession. Magn Reson Med 2006;55: 557–565.
14. Nayak KS, Lee HL, Hargreaves BA, Hu BS. Wideband SSFP: alternating repetition time balanced steady state free precession with increased band spacing. Magn Reson Med 2007;58:931–938.
15. Lee HL, Pohost GM, Nayak KS. Gated and real-time wideband SSFP cardiac imaging at 3t. In: Proceedings of the 14th Annual Meeting of ISMRM, Seattle, 2006. (abstract 143).
16. Deshpande VS, Shea SM, Li D. Artifact reduction in True-FISP imaging of the coronary arteries by adjusting imaging frequency. Magn Reson Med 2003;49:803–809.
17. Hargreaves BA, Vasanawala SS, Pauly JM, Nishimura DG. Characterization and reduction of the transient response in steady-state MR imaging. Magn Reson Med 2001;46:149–158.
18. Nguyen TD, Spincemaille P, Prince MR, Wang Y. Cardiac fat navigator-gated steady-state free precession 3D magnetic resonance angiography of coronary arteries. Magn Reson Med 2006;56:210–215.
19. LeRoux P. Simplified model and stabilization of SSFP sequences. J Magn Reson 2003;163:23–37.
20. Lee HL, Nayak KS. Stabilization of alternating TR steady state free precession sequences. J Magn Reson 2008;195:211–218.
21. Markl M, Alley MT, Elkins CJ, Pelc NJ. Flow effects in balanced steady state free precession imaging. Magn Reson Med 2003;50:892–903.
22. Sodickson DK, Manning WJ. Simultaneous acquisition of spatial harmonics (SMASH): fast imaging with radiofrequency coil arrays. Magn Reson Med 1997;38:591–603.
23. Pruessmann KP, Weiger M, Scheidegger MB, Boesiger P. SENSE: sensitivity encoding for fast MRI. Magn Reson Med 1999;42: 952–962.
24. Griswold MA, Jakob PM, Heidemann RM, et al. Generalized autocalibrating partially parallel acquisitions (GRAPPA). Magn Reson Med 2002;47:1202–1210.
25. Lee H-L, Kim Y-C, Shankaranarayanam A, Nayak KS. Auto-calibrated parallel imaging using the unused echo in alternating TR SSFP. In: Proceedings of the 17th Annual Meeting of ISMRM, Honolulu, 2009. (abstract 768).
26. Lee H-L, Kim Y-C, Shankaranarayanam A, Nayak KS. Retrospective self-navigated cine imaging using the unused echo in alternating TR SSFP. In: Proceedings of the 17th Annual Meeting of ISMRM, Honolulu, 2009. (abstract 4643).
27. Larson AC, White RD, Laub G, McVeigh ER, Li D, Simonetti OP. Self-gated cardiac cine MRI. Magn Reson Med 2004;51:93–102.
28. Fung MM, Ho VB, Hood MN, Schmidt EJ. Multi-phase fat-suppressed 3D SSFP for robust coronary artery imaging: improvements over the single phase technique. In: Proceedings of the 16th Annual Meeting of ISMRM, Toronto, 2008. (abstract 313).
29. Cheng A, Pegg T, Karamitsos T, et al. Cardiovascular magnetic resonance perfusion imaging at 3-tesla for the detection of coronary artery disease: a comparison with 1.5-Tesla. J Am Coll Cardiol 2007;49:2440–2449.
30. Gutberlet M, Schwinge K, Freyhardt P, et al. Influence of high magnetic field strengths and parallel acquisition strategies on image quality in cardiac 2d cine magnetic resonance imaging: comparison of 1.5 t vs. 3.0 t. Eur Radiol 2005;15:1586–1597.
31. Brittain JH, Hu BS, Wright GA, Meyer CH, Macovski A, Nishimura DG. Coronary angiography with magnetization-prepared T2 contrast. Magn Reson Med 1995;33:689–696.